AERODYNAMIC PERFORMANCE AND BOUNDARY LAYER GROWTH ON ROUGH SYMMETRICAL AIRFOIL AT LOW-REYNOLDS NUMBERS

H.A. Abdalla, A.M. Alam El-Din, T.I. Sabry and S.R. Ismail

Department of Mechanical Power Engineering, Faculty of Engineering,
Menoufia University, Shebin El-Kom, Egypt.

ABSTRACT

This paper reports the results of an experimental investigation on the aerodynamic performance and flow structures over smooth and rough airfoils at low-Reynolds number. The airfoil surface was roughened using three kinds of sand papers have different arithmetic center-line average roughness (RA). Experiments included measurements of the static pressure distributions, the streamwise boundary layer mean-velocity profiles and the skin friction coefficient was determined by Clauser method. The corresponding aerodynamic parameters such as lift and drag coefficients are measured for the same testing conditions. Data indicated that, the boundary layer properties are found to be strongly dependent on the surface roughness. The presence of surface roughness causes a distortion in the velocity profiles past airfoils. It is found that, the hysteresis phenomenon in the lift coefficient-curves of both smooth and rough airfoils is strongly affected by the surface roughness and the operated Reynolds number. Hysteresis is of practical importance because it results in producing different aerodynamic performance. Moreover, the angle of zero-lift is partically unaffected by the surface roughness. The operating range of rough airfoils is limited by stall and separation at low angles of attack.

Key words: Airfoil, Aerodynamic parameters, Boundary layer, Separation, Roughness, Reynolds number.

Nomenclature

C	airfoil chord
C_D	drag coefficient
C_f	skin-friction coefficient
C_L	lift coefficient
C_P	static-pressure coefficient, $(p-p_\infty)/(\rho U_\infty^2/2)$
H	boundary layer shape factor, δ^* / θ
P	static pressure
RA	arithmetic center-line average roughness
R_c	Reynolds number, $U_\infty C /\upsilon$
U_∞	free-stream velocity
u^*	shear velocity, $(\tau_w/\rho)^{0.5}$
u	fluid-velocity parallel to airfoil surface
U^+	the dimensionless velocity, u / u^*
X	streamwise-direction along the chord line, with origin at the leading edge
y	crosswise-direction normal to the chord line
y^+	the dimensionless normal distance, $y u^* / \upsilon$
α	angle of attack
δ	boundary layer thickness, value of y at which $u = 0.99 U_\infty$
δ^*	boundary layer displacement thickness, $\int_0^\delta (1 - \frac{u}{U_\infty})dy$
θ	boundary layer momentum thickness, $\int_0^\delta (1 - \frac{u}{U_\infty})\frac{u}{U_\infty}dy$
υ	kinematic viscosity

Subscripts

cr	critical conditions
max	maximum conditions
∞	free-stream value

1- INTRODUCTION

There are many applications where turbulent boundary layers over longitudinally rough curved surfaces are encountered. Some examples are blade passages of turbomachinery, airfoils and hub of propellers. Most of these applications are usually manufacture by casting and the wall surface is usually not aerodynamically smooth. Traditionally, such boundary layers have been studied ignoring surface roughness effects, Ref. [1] to Ref. [4]. However, it is expected that the boundary layer development over the curved surface is very sensitive to the surface roughness. Previously, experiments have shown that, various roughness types have effects on boundary layer growth and transition process. Many parameters such as the roughness height, shape, density and manner of distribution are important in determining the net effect of the roughness on the boundary layer growth; Ref. [5] to Ref. [9]. A few investigations along these lines were reported recently to examine the effect of surface roughness on both the onset and length of the transition region, Ref. [10] and Ref. [11]. In the pervious studies, it was found that a number of factors combine to determine the onset and length of the transition region. Two important ones are the streamwise pressure gradient and the free stream turbulence level, Ref. [12] and Ref.[13]. It appeared also from the literature review that, models of transition process are not adequate and more experimental data that might provide guidelines for improving these models regarding the roughness effect are needed. This is useful for investigating the aerodynamic properties and the flow structures on airfoils and curved surfaces which have drawn much attention in recent years. Therefore, this investigation aims to study the flow characteristics and the boundary layer growth past rough airfoil surfaces.

The understanding of the boundary layer development over airfoils, especially in the presence of surface roughness and pressure gradient, is important for determining the aerodynamic characteristics as well as the operational conditions of airfoils. The growth and separation of the boundary layer which form on airfoils govern the airfoil stall conditions. The nature and the extent of separated regions are determined primarily by the airfoil shape, the angle of attack, the flow parameters such as the pressure gradient ,the Reynolds number and the free stream turbulence. The flow behavior past an airfoil can be described as follows. The flow in the vicinity of the leading edge of an airfoil subject to leading-edge separation. The laminar boundary layer, extending from the stagnation point over the leading edge, and may separate just downstream of the point of minimum pressure, Ref. [14] to Ref. [18]. Transition to turbulent flow occurs in the free-shear layer a short distance downstream of the separation point. The flow then reattach to the airfoil surface, with a turbulent boundary layer extending from the reattachment point to the trailing edge, as shown in Figure (1). If the angle of attack of airfoil is increased, the laminar-separation bubble moves closer to the leading edge and becomes slightly shorter. Although a lot of available experimented data in the literature survey on the flow and friction loss of rough wall pipes and flat plates, a few experimental investigations are available for flows past rough curved surfaces, such as presented in Ref. [19] and Ref. [20]. It appears from the literature survey that, the combined effect of the surface curvature and the surface roughness is not clarified. However, roughness elements such as trip-wires were used to study the effect of rough surface on the stability of the boundary layer past a flat plate at different incidence angles, Ref. [21] and Ref. [22]. It was found that, leading-edge separation occurs due to the wake of the trip wires located at the leading edge of the plate and due to the incidence angle.

This investigation reports mainly the results pertaining to roughness effects on the behavior of the mean flow and aerodynamic characteristics of a model with NACA-0012 airfoil at a low-Reynolds number which ranging from $2x10^5$ to $3.37x10^5$. The experiments are conducted for smooth and rough airfoils. The airfoil is roughened using three kinds of sand papers. The measured arithmetic center-line average roughness (RA) for the sand papers are $1x10^{-2}$, $2.85x10^{-2}$ and $7.125x10^{-2}$ mm. The measurements are carried out for the static pressure distributions and the streamwise boundary layer mean velocity profiles. The corresponding aerodynamic parameters such as lift and drag coefficients are measured for the same testing conditions.

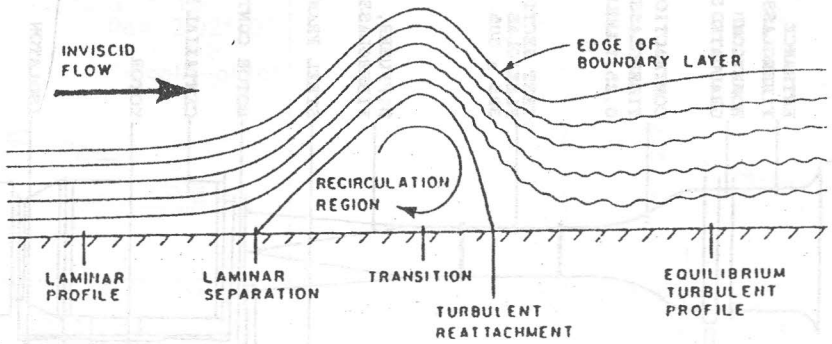

Figure 1. Structure of laminar separation bubble.

2- EXPERIMENTAL APPARATUS AND INSTRUMENTATION

The experiments were carried out in a low turbulence open-type wind tunnel. The wind tunnel employed in these experiments is shown in Figure (2). It consists of six parts centeraxial fan, wide angle diffuser, test section, contraction with 0.25 to 1.0 diameter ratio, settling chamber and the entrance portion. All the wind tunnel, except the fan, is made of fiberglass and fixed on a movable steel frame. Honeycomb and graduated screens are installed in the settling chamber for breaking the free-stream turbulence which is less than 0.05% at air velocity of 55 m/s. The control panel of the wind tunnel consists of a variable frequency controller and a remote speed control device. The air speed in the test section can be controlled from the control panel of the wind tunnel using a pre-calibrated curve. Calibration for the wind tunnel air speed against the frequency of the wind tunnel variable frequency controller was made using a pitot-tube and a pressure transducer. The pressure was converted into speed and a straight line relation between the air speed and the frequency was obtained. The test section, which is made of prespex, has a square cross-section 305x305 mm and 610 mm long. At the top wall of the test section, a traversing unit was mounted and a small slot in the longitudinal direction was made to accommodate the probe holder. The area of the slot around the probe holder was sealed to prevent disturbance to the flow by leakage.

The airfoil model is horizontally mounted by a vertical adjustable strut in the test section and airfoil cross-section is a NACA-0012 airfoil. The strut allows the airfoil to be inclined with the desired angle of attack. The chord of the model is 100 mm and its span is 300 mm. It is manufactured to accommodate nine taps staggered along the chordwise direction at the mid-span of the model. The taps are drilled normal to the model surface. The internal diameter of each tap is about 1 mm. The smooth airfoil surface is made of a filled epoxy resin. To study the effect of surface roughness, the airfoil surface was roughened using three kinds of the sand papers which were different in the roughness degree. The measured arithmetic center-line average roughness (RA) of the sand-grain papers are $1x10^{-2}$ mm, 2.85×10^{-2} mm and $7.125x10^{-2}$ mm, which are designated as RA1, RA2 and RA3, respectively. The thickness of the sand papers is taken into account during the fabrication of the tested rough airfoils to prevent any change in the airfoil dimensions.

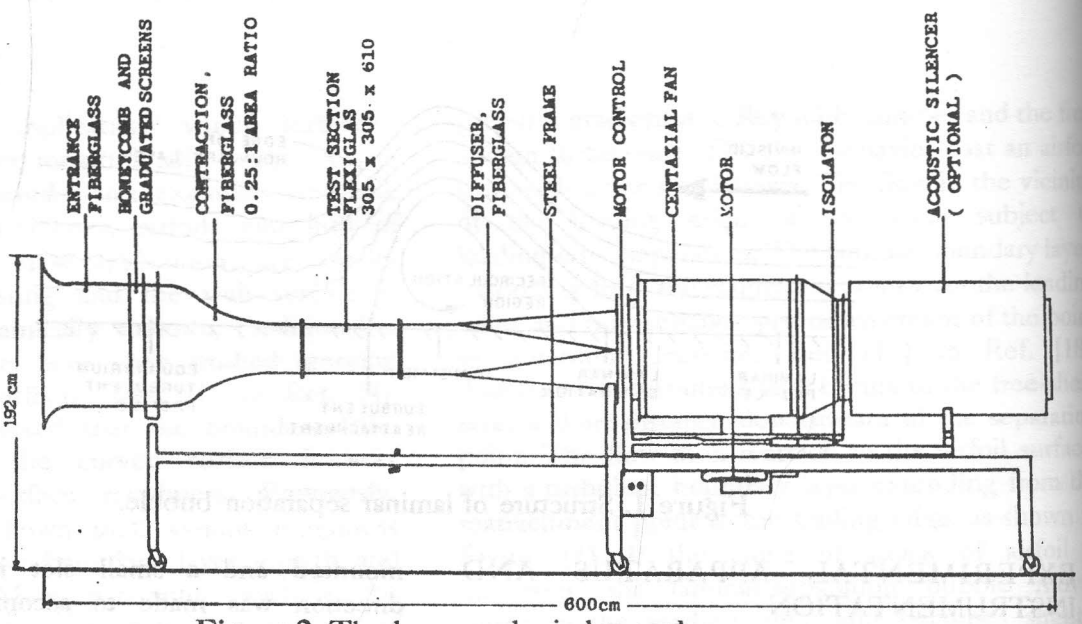

Figure 2. The low-speed wind tunnel.

Measurements were acquired for the mean velocity-profiles in the streamwise direction at an angle of attack of 0, 5 and 10 degrees for smooth and sand-grain roughness type. A calibrated five-holes probe was used to measure the boundary layer mean velocity profiles along the airfoil chord. The boundary layer momentum thickness, θ, and the displacement thickness, δ^*, as well as the shape factors, H, were obtained from the measured velocity profiles at different locations past the tested airfoils. The chordwise static pressure distributions were measured using sensitive pressure transducers. In addition, the wall shear stress and hence the skin friction coefficient was determined by the Clauser method [23]. Besides the mean flow parameters, the aerodynamic characteristics of the tested models were measured at different angles of attack ranging from -15 to 20 degrees. The lift and drag forces which give the airfoil performance were measured using the calibrated lift and drag dynamometer. The measurements of mean-velocity profiles are conducted at Reynolds number of 2.02×10^5, while the measurements of pressure distribution and lift and drag coefficients are carried out at different Reynolds numbers, Re = 2.02×10^5 to 3.37×10^5. The Reynolds number is based on the free-stream velocity and the airfoil chord.

The experiments showed that the error in the mean velocity measurements by the five-holes probe is about $\pm$ 1% at the maximum calibration velocity of 50 m/s. The error in the static pressure measurements is about $\pm$ 0.5%. The uncertainty in the experimental results were calculated using Kline and Mcclintock technique [24].

3- EXPERIMENTAL RESULTS

3-1 *Pressure Distribution and Reattachment Point*

The chordwise distributions of the pressure coefficient, Cp, past the upper surfaces of smooth and rough airfoils are shown in Figure (3) to Figure (6) for angles of attack of 0, 5, and 10 degrees. For zero-angle of attack and for both smooth and rough airfoil surfaces, these figures indicate that the pressure coefficient decreases from positive value near the leading edge to a minimum negative value for a distance along the airfoil chord and then an adverse pressure gradient appears and extends up to the trailing edge. In general, the pressure distributions indicate that the flow remains laminar from the leading edge to the minimum pressure point and then the process of transition to turbulent flow occurs when the pressure gradient becomes positive. Increasing the angle of attack or the surface roughness moves the location of the minimum pressure point towards the leading edge and the resultant pressure distribution varies sharply near the leading edge, i.e. there are large negative values of Cp. The sharper the variations, the stronger the adverse pressure gradient imposed on the boundary layer after the minimum pressure point. This increases the form drag due to friction and may also lead to boundary layer separation.

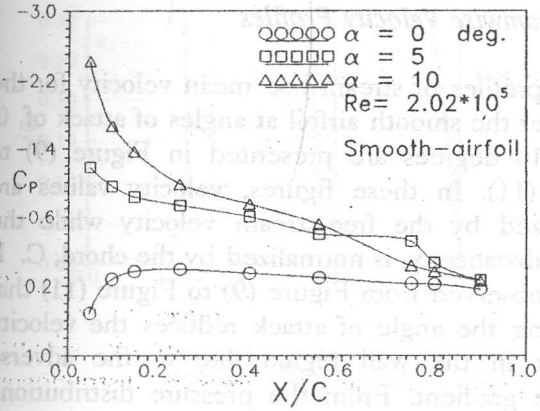

Figure 3. Effect of angle of attack on C_p-distribution of smooth airfoil.

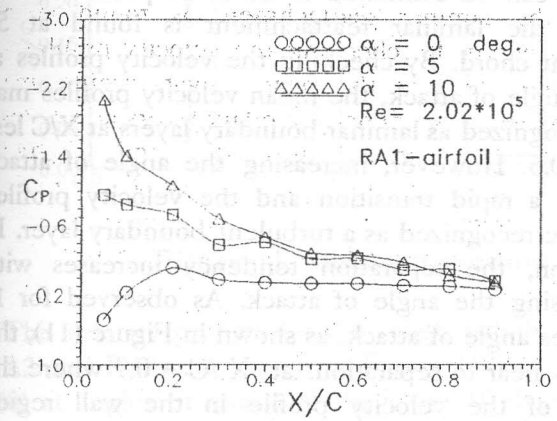

Figure 4. Effect of angle of attack on C_p-distribution of RA1-airfoil.

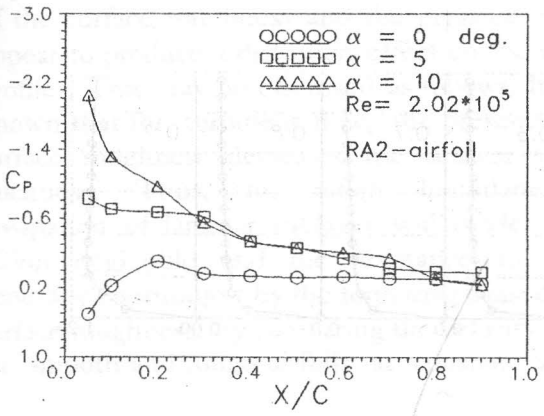

Figure 5. Effect of angle of attack on C_p-distribution of RA2- airfoil.

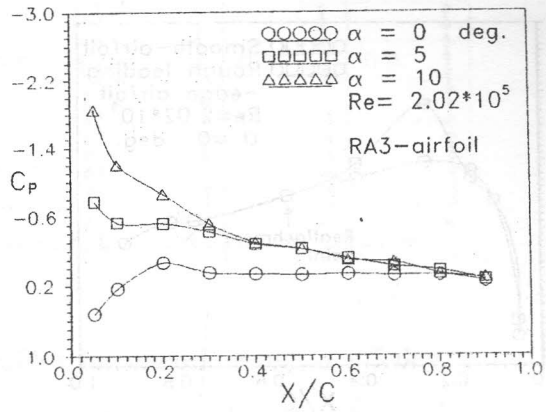

Figure 6. Effect of angle of attack on C_p-distribution of RA3 airfoil.

If the separation occurs in the laminar flow near the leading edge, early transition to turbulent flow may follow, and the separated flow will reattach due to the higher rate of momentum transport with turbulent boundary layer. Therefore, it is felt that the transition point and the length of transition zone may play an important role in the separation of the turbulent boundary layer. In order to find the reattachment point, a rough strip of sand paper is located at the leading edge to suppress the laminar separation. It is suggested that the reattachment occurs when the pressure is nearly equal to the value for the turbulent boundary layer over the airfoil with no-laminar separation present. Results of the measured pressure distribution for smooth and rough leading edge airfoils are plotted in Figure (7) and Figure (8) for angles of attack of zero and 5 degrees. For zero-angle of attack, it is observed that two sets of pressure distributions coinside with each other at 55 % chord, then they move to 40% chord when the angle of attack is increased to 5 degrees. Therefore, it can be concluded that the reattachment point of the laminar boundary layer moves towards the leading edge with increasing the angle of attack due to the creation of an adverse pressure gradient, so that the result is an effective thickening of the upper surface near the leading edge. Consequently, the length of the transition zone and stalling condition are strongly affected by the angle of attack and the surface roughness. The pressure distributions along with the boundary layer velocity profiles can be used to study the process of transition from laminar to turbulent flow. The details will be described in the following sections.

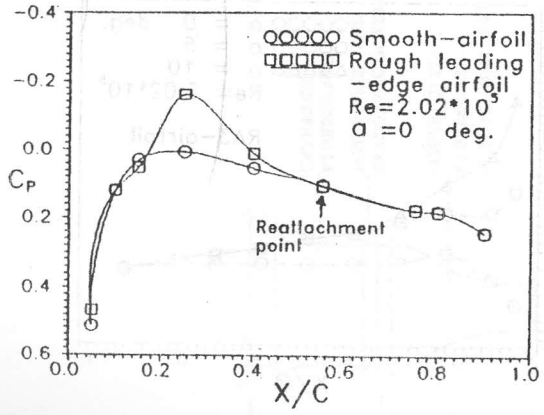

Figure 7. Chordwise pressure distribution for smooth and roughened leading-edge airfoil.

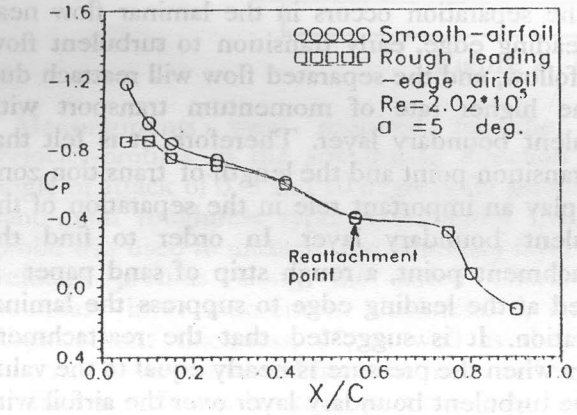

Figure 8. Chordwise pressure distribution for smooth and roughened leading-edge airfoil.

3-2 *Streamwise Velocity Profiles*

The profiles of streamwise mean velocity for the flow over the smooth airfoil at angles of attack of 0, 5 and 10 degrees are presented in Figure (9) to Figure (11). In these figures, velocity values are normalized by the free-stream velocity while the normal distance, y, is normalized by the chord, C. It can be observed from Figure (9) to Figure (11) that increasing the angle of attack reduces the velocity gradient in the wall region due to the adverse pressure gradient. From the pressure distributions along the chord-wise direction at zero angle of attack, the transition point (minimum pressure point) can be estimated to be at 26 percent chord while the laminar reattachment is found at 55 percent chord. By checking the velocity profiles at zero-angle of attack, the mean velocity profiles may be recognized as laminar boundary layers at X/C less than 0.5. However, increasing the angle of attack causes a rapid transition and the velocity profiles may be recognized as a turbulent boundary layer. In addition, the separation tendency increases with increasing the angle of attack. As observed for 10 degrees angle of attack, as shown in Figure (11), the flow is near to separation. at X /C = 0.9 where the slope of the velocity profile in the wall region becomes steeper.

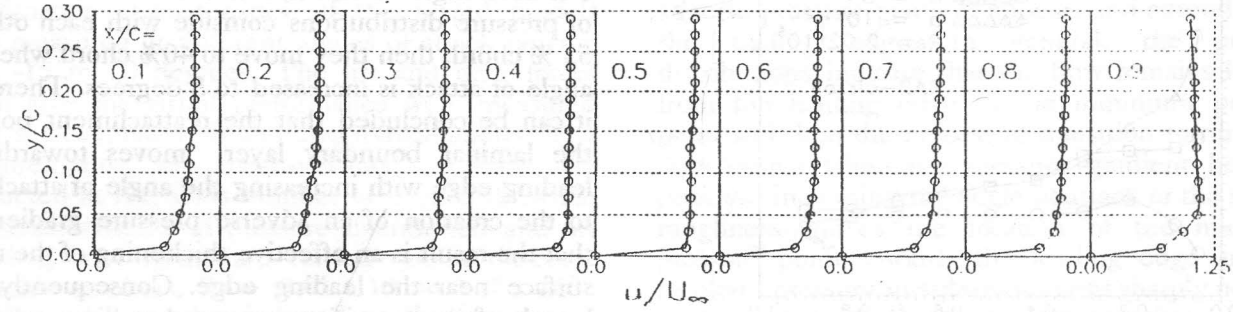

Figure 9. Measured streamwise velocity-profiles for smooth airfoil, α = 0 deg.

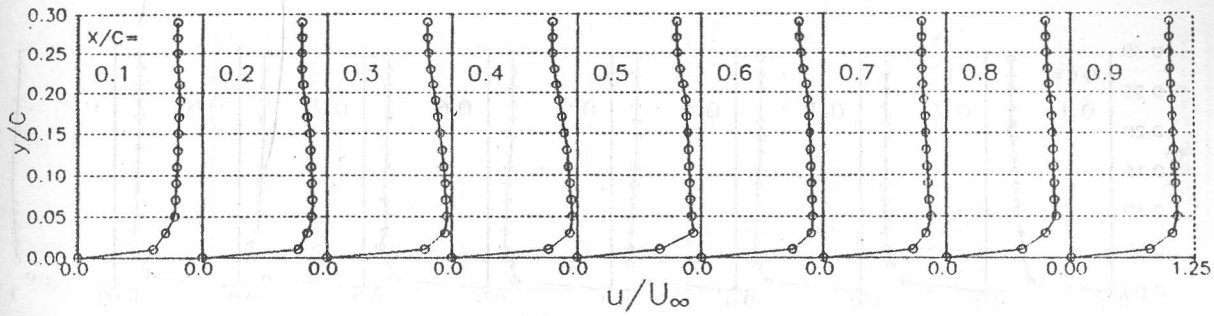

Figure 10. Measured streamwise velocity-profiles for smooth airfoil, α = 5 deg.

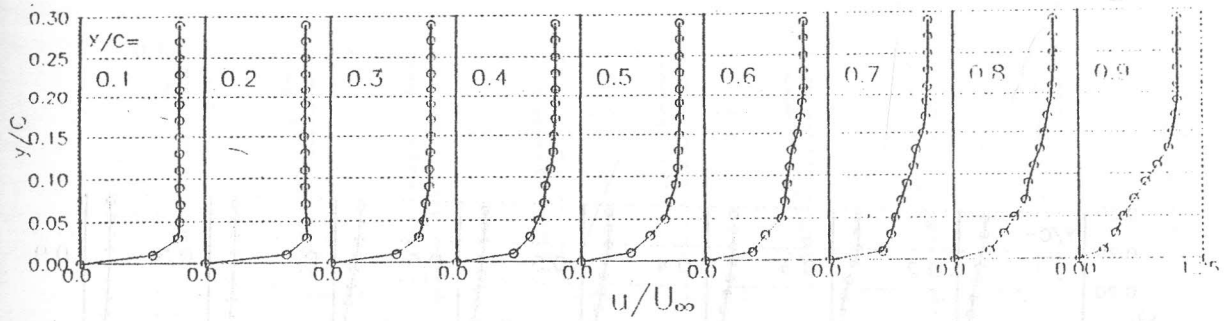

Figure 11. Measured streamwise velocity-profiles for smooth airfoil, α = 10 deg.

The velocity profiles for the rough airfoils (RA1, RA2 and RA3) are shown in Figure (12) to Figure (20) at angles of attack of 0, 5 and 10 degree. In general, the velocity profiles over rough airfoils are recognized as turbulent boundary layer and indicate that the velocity values near the wall are strongly dependent on the surface roughness. The presence of the surface roughness and the pressure gradient appear to produce a distortion effect on the velocity profiles. This may be discussed as follows. It is well known that for turbulent flow, the presence of the surface roughness decreases the laminar sublayer thickness. Thus, for rough boundaries, the dissipation of laminar sublayer will render viscous action negligible and the resistance to flow is generally contributed by the form drag caused by the surface roughness. By comparing the velocity profiles for smooth and rough airfoils at constant angle of attack, it can be observed that, the velocity values in the wall regions increase with increasing the surface roughness and the maximum velocity is shifted towards the wall region, as observed for angle of attack of zero and 5 degrees. On the other hand, the velocity gradients of rough airfoils become more steeper than that of smooth airfoil surface. However, increasing the surface roughness at 10 degrees angle of attack tends to decelerate the flow and results in more steeper velocity profiles and the flow separation occurs earlier. As shown in Figures (14), (17) and (20), the separation position moves in the upstream direction as the surface roughness increases. This may be due to that, the fluid in the wall region has to do work against friction and work against increasing pressure gradient. Accordingly, the total drag increases and hence the boundary layer thickness increases and tends to separate from the airfoil surface even earlier.

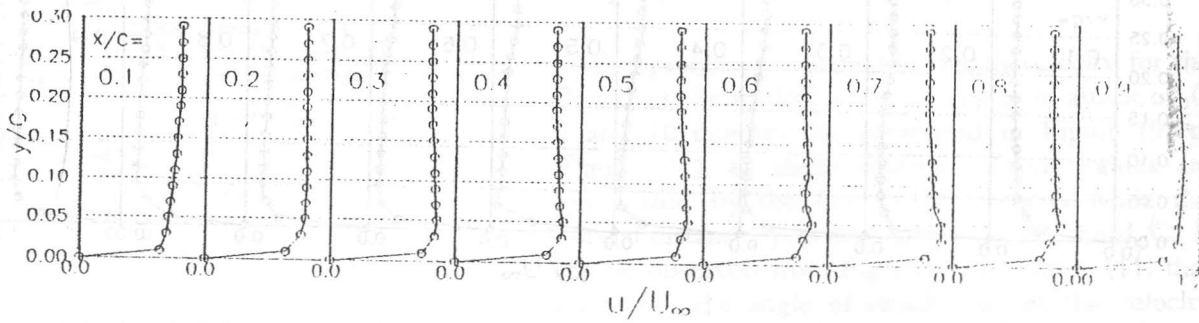

Figure 12. Measured streamwise velocity-profiles for RA1-airfoil, α = 0 deg.

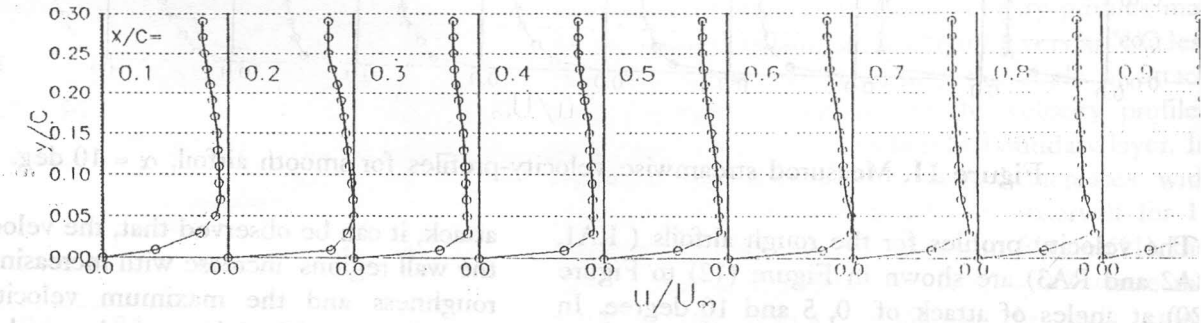

Figure 13. Measured streamwise velocity-profiles for RA1-airfoil, α = 5 deg.

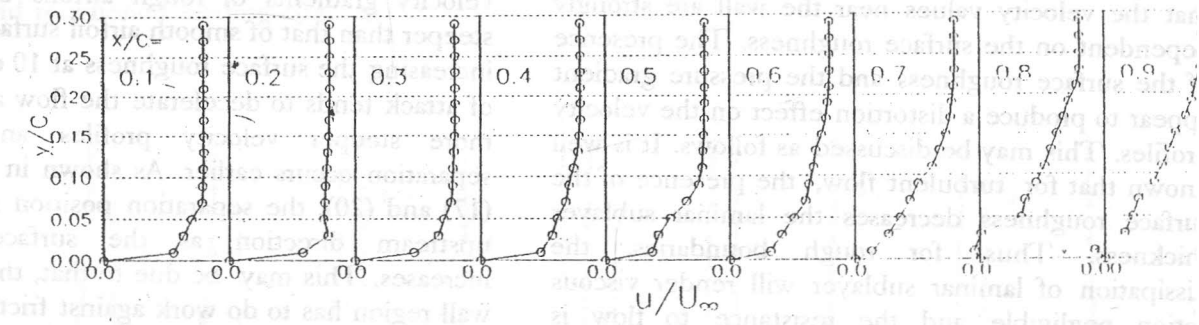

Figure 14. Measured streamwise velocity-profiles for RA1-airfoil, α = 10 deg.

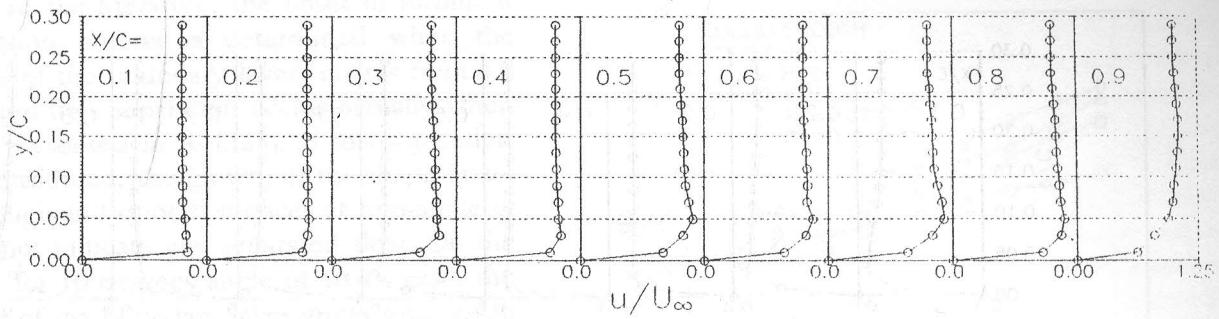

Figure 15. Measured streamwise velocity-profiles for RA2-airfoil, α = 0 deg.

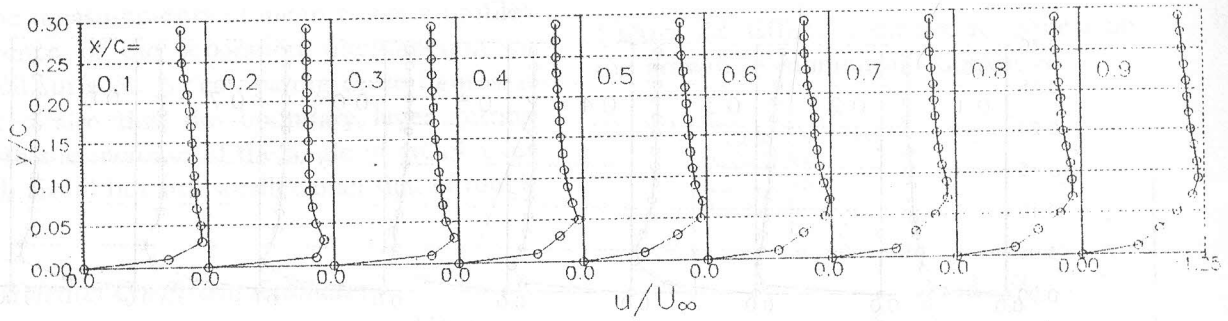

Figure 16. Measured streamwise velocity-profiles for RA2-airfoil, α = 5 deg.

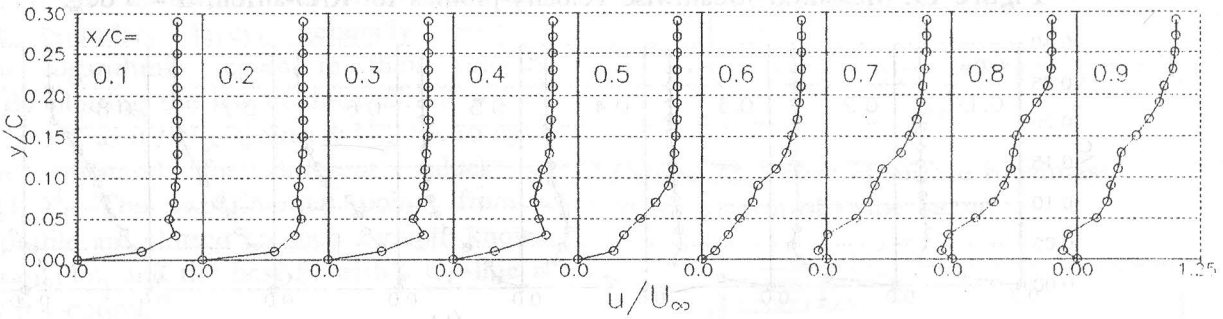

Figure 17. Measured streamwise velocity-profiles for RA2-airfoil, α = 10 deg.

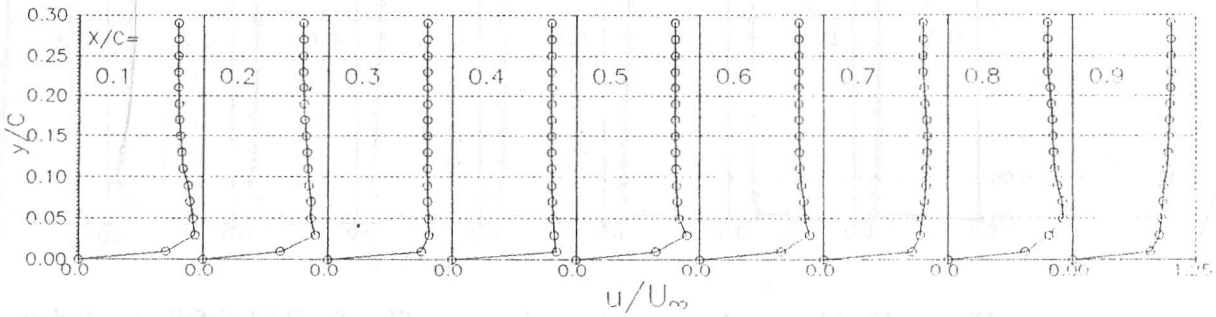

Figure 18. Measured streamwise velocity-profiles for RA3-airfoil, α = 0 deg.

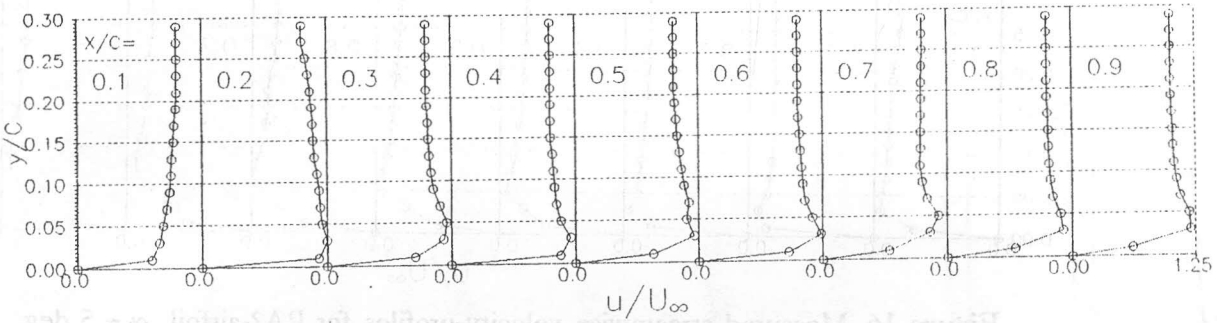

Figure 19. Measured streamwise velocity-profiles for RA3-airfoil, α = 5 deg.

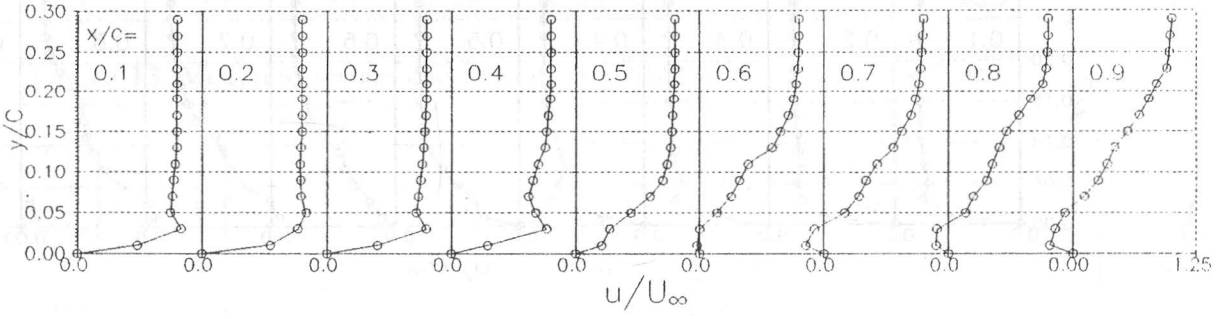

Figure 20. Measured streamwise velocity-profiles for RA3-airfoil, α = 10 deg.

3-3 *Boundary-Layer Integral Parameters*

The variations of the momentum thickness, θ, the displacement thickness, δ^*, and the shape factor, H, which are known as the boundary layer integral parameters, with the chordwise direction are shown in Figure (21) to Figure (26). Figure (21) to Figure (23) illustrate the boundary layer parameters for smooth and rough airfoil surfaces at zero-angle of attack, while Figure (24) to Figure (26) indicate the results at 10 degrees angle of attack. It can be observed that the effect of surface roughness on the boundary layer growth is to increase the values of the displacement thickness and the momentum thickness rapidly compared to those of the smooth airfoil surface. In turn, the effect of roughness on velocity distributions is reflected in a raising of the shape factor, H. It can be seen clearly for zero-angle of attack that, the boundary layer parameters increase linearly except at the stations near to the leading edge. This may be due to the transition from laminar to turbulent flow, as discussed

previously. In the literature, the onset of turbulent flow separation criteria is determined when the shape factor of the boundary layer ranges from 1.8 to 2.4, but the flow separation occurs actually when H = 2.6 as presented in Ref.[25]. If this separation criteria is considered, the growth of the shape factor along the rough and smooth surfaces at zero-angle of attack will not indicate any separated flow. On the other hand, for 10 degrees angle of attack case, the shape factor of the boundary layer grows over rough airfoil more rapidly and hence the flow separates earlier due to the presence of a strong adverse pressure gradient. The values of the shape factor confirm the measurements of mean velocity profiles for occurrence of the separation phenomenon on rough airfoil surfaces. By comparing these figures, it can be seen also that the boundary layer getting thicker with the increase of the angle of attack over the smooth airfoil but still smaller than that of rough airfoils.

3-4 *Skin-Friction Coefficient Estimates*

The skin-friction coefficient, C_f, however, may be found indirectly by making use of the fact that turbulent boundary layers generally have a significant logarithmic region in their velocity profiles. By plotting the law of the wall, $U^+ = 5.75 \log 10\ y^+ + 5.5$, as u / U_∞ against $y U_\infty / \nu$, straight lines are obtained for different values of $C_f = 2(u^*/U_\infty)^2$. The experimental points from a velocity profile are plotted on such a graph, known as a Clauser plot, and the best fit with a C_f -line is found by inspection.

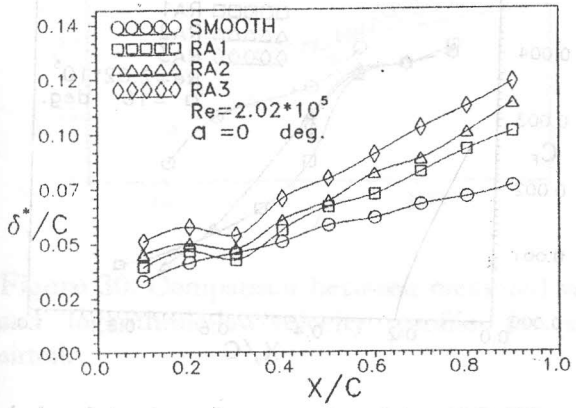

Figure 21. Effect of surface roughness on the growth of displacement thickness.

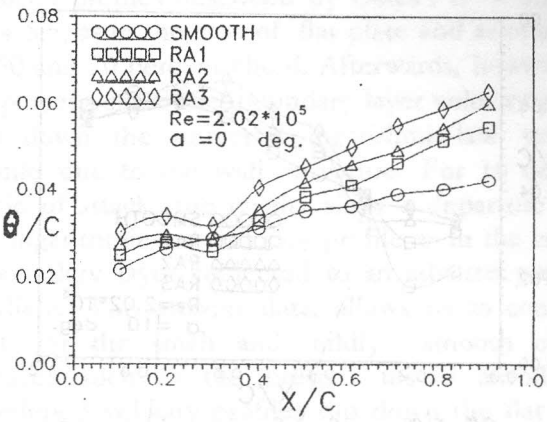

Figure 22. Effect of surface roughness on the growth of momentum thickness.

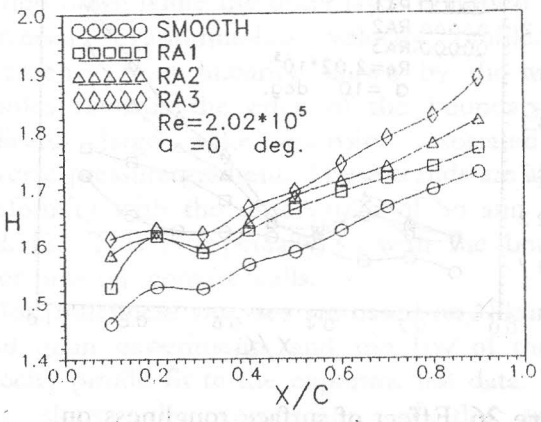

Figure 23. Effect of surface roughness on the growth of shape factor.

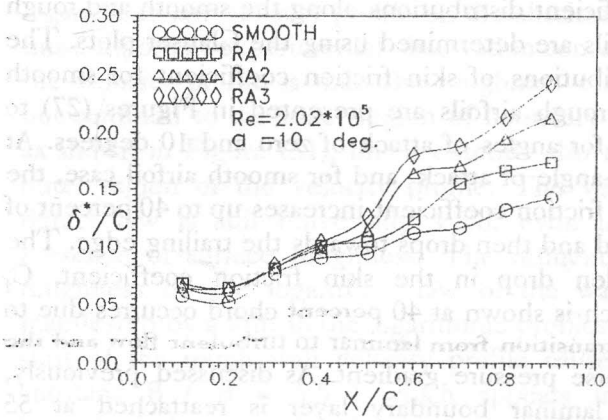

Figure 24. Effect of surface roughness on the growth of displacement thickness.

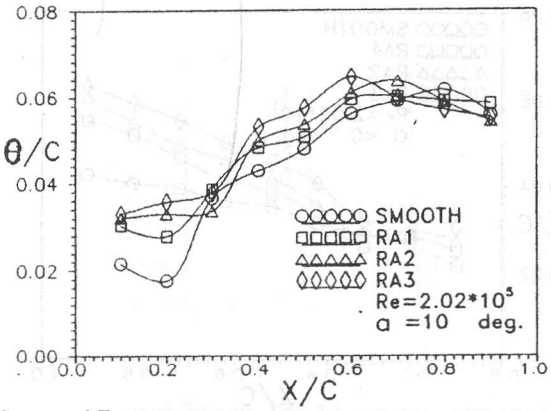

Figure 25. Effect of surface roughness on the growth of momentum thickness.

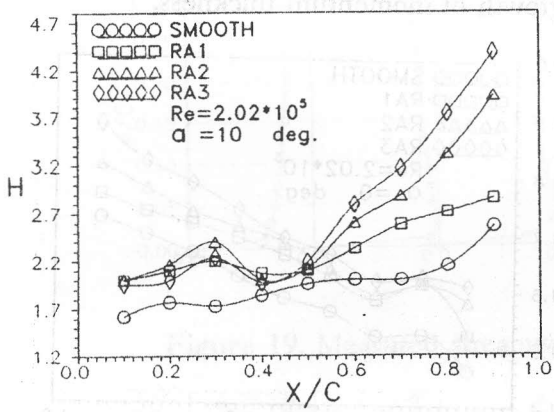

Figure 26. Effect of surface roughness on the growth of shape factor.

In the present work, the local skin-friction coefficient distributions along the smooth and rough airfoils are determined using the Clauser plots. The distributions of skin friction coefficient for smooth and rough airfoils are presented in Figures (27) to (28) for angles of attack of zero and 10 degrees. At zero-angle of attack and for smooth airfoil case, the skin friction coefficient increases up to 40 percent of chord and then drops towards the trailing edge. The sudden drop in the skin friction coefficient, C_f ,which is shown at 40 percent chord occurres due to the transition from laminar to turbulent flow and the adverse pressure gradient. As discussed previously, the laminar boundary layer is reattached at 55 percent chord after transition. This confirms the results of the skin friction coefficient distribution. In general, the effect of increasing the surface roughness on the skin friction coefficient in the case of zero-angle of attack appears clearly to increase the values of the skin-friction coefficient. Increasing the angle of attack from zero to 10 degrees tends to decrease the values of the skin friction coefficient of rough airfoils due to the creation of an adverse pressure gradient. At 10 degrees angle of attack, the skin friction coefficient of smooth airfoil does not reach zero value on the airfoil surface which leads to non separated flow. On the other hand, increasing the surface roughness lowers the values of the skin friction coefficient and approachs near to zero values in the region of separated flow. Therefore, it can be concluded that, increasing the surface roughness in zero pressure gradient tends to increase the skin friction coefficient at constant Reynolds number, but it is decreased in the presence of adverse pressure gradient due to the separation possibility.

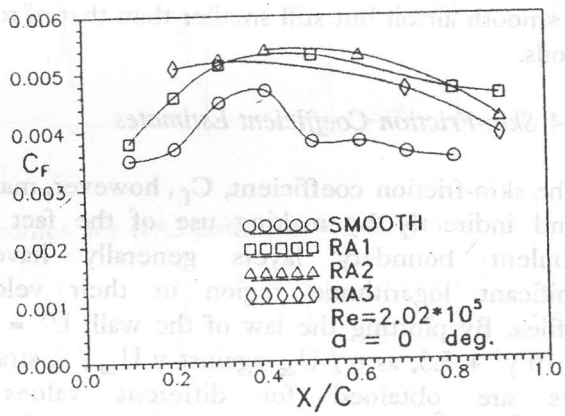

Figure 27. Effect of surface roughness on chordwise skin-friction distribution.

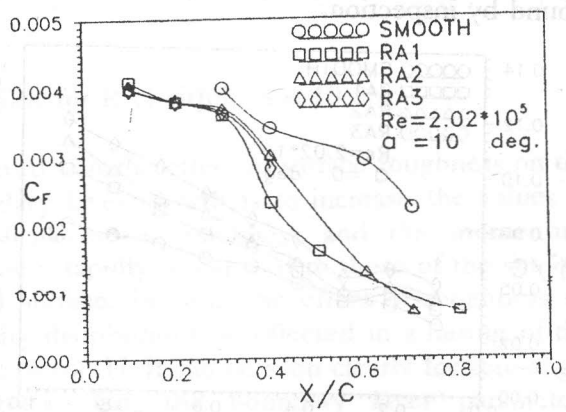

Figure 28. Effect of surface roughness on chordwise skin-friction distribution.

Here, to study the effect of wall roughness on the mean velocity profiles of the inner layer in the wall boundary layer developed on the rough airfoils, the mean velocity profiles, are presented in terms of the inner variables which are known as the shear velocity, u^*, and the dimensionless distance from the wall, $y^+ = y\, u^*/ \nu$. Firstly, to check the values obtained of skin friction coefficient, samples of the developed velocity profiles on the smooth airfoil are plotted in Figure (29) and Figure (30) at locations of 50,70 and 90 percent chord at zero and 10 degrees angle of attack.

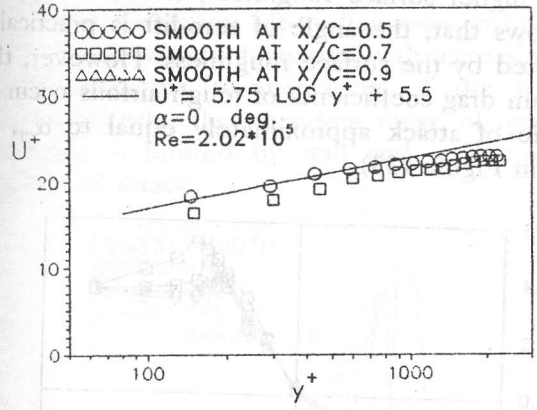

Figure 29. Comparison between measured velocity and boundary layer universal velocity profile for smooth airfoil.

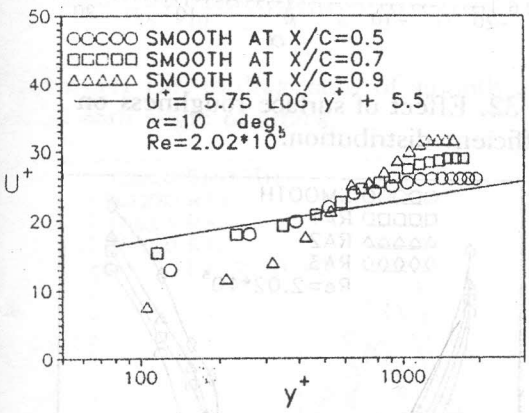

Figure 30. Comparison between measured velocity and logarithmic-law-velocity profile for smooth airfoil.

It can be seen for zero-angle of attack that, the experimental data agrees with the logarithmic-law of velocity profiles described by Coles : $U^+ = 5.75 \log y^+ + 5.5$, as in the case of flat plate and as observed at 50 and 70 percent chord. Afterwards, however, at 90 percent chord the boundary layer velocity profile dip down the universal logarithmic-law velocity profile due to the wall curvature. For 10 degrees angle of attack, the results show a departure from the logarithmic-law velocity profile as in the case of a boundary layer subjected to an adverse pressure gradient. The present data, allows us to conclude that, for the small and mildly smooth curved surfaces such as the present tested airfoil, the developed velocity profiles dip down the flat plate boundary layer (zero-pressure gradient). However, in the presence of pressure gradient, the inner layer of the developed velocity profile on smooth airfoil is shifted down while the outer layer is shifted up the universal logarithmic-law velocity profile. The divergence from linearity shown by the velocity profiles towards the edge of the boundary layer indicates large wake intensity associated with adverse pressure gradient. These trends are again in conformity with the observation of So and Mellor Ref. [2]. This is especially so with the boundary layer flow on convex walls.

Most roughness analyses are based on Nikuradse's sand grain experiments and the law of the wall velocity profile fit to the experimental data. Figure (31) shows the comparison of the velocity distribution between the smooth and the rough walls at zero-angle of attack. It is observed from this figure that the roughness will shift down the logarithmic-law velocity profile on the abscissa. The most important experimental observation concerning the velocity profile is that, the roughness effect is not confined to the inner region of boundary layer, as shown in Figure (31), but it extends also to the outer region of the velocity profile. The velocity defect law is still universally valid, even in the presence of surface roughness. The influences of roughness on the logarithmic-law of the wall are manifested by a shift in the logarithmic profiles. The shift of the rough wall velocity profile causes the constant B (B = 5.5) which appears in the logarithmic law to be less by an amount ΔB. This is obtained previously by Nikuradse. On the other hand, the outer layer of the boundary layer is affected significantly by the wall roughness, as

shown in Figure (31). Therefore, the departure from the logarithmic-law increases compared to the smooth airfoil case due to the combined effects of wall curvature and the surface roughness.

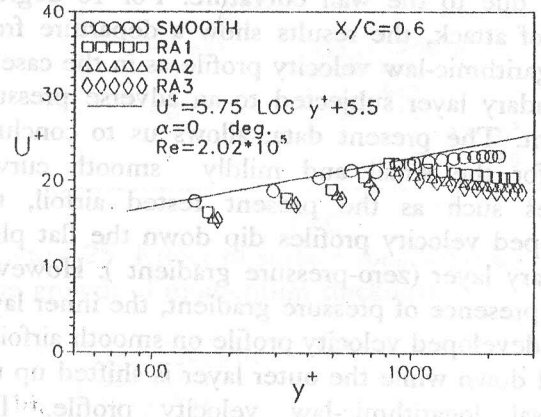

Figure 31. Effect of surface roughness on boundary layer universal velocity profile.

3-5 *Aerodynamic Characteristics*

The variations of lift coefficient, C_L, and the drag coefficient, C_D, with the angle of attack, α, for rough airfoil surfaces are shown in Figure (32) and Figure (33) compared with those of smooth airfoil. It is observed that at low-to- moderate angle of attack, the lift coefficient varies linearly with the angle of attack. In this region, the flow moves smoothly over the airfoil and is attached over most of the surface. However, as the angle of attack becomes large, the flow tends to separate from the upper surface of the airfoil, creating a large wake behind the airfoil. The consequence of this separated flow at high angle of attack is a precipitous decrease in the lift and rapid increase in drag. Under such conditions, the airfoil is said to be stalled. The maximum value of C_L, which occurs just prior to the stall, is denoted by $C_{L\ max}$. The value of α when lift equal a maximum value is called the critical angle of attack, α_{cr}. The C_{Lmax} is one of the most important aspects of airfoil performance. The higher the C_{Lmax}, the lower is the stalling speed. Again examining these figures, it can be seen that the lift coefficient increases linearly with the angle of attack until flow separation begins to have an effect, then the variation becomes nonlinear, C_L reaches a maximum value, and finally the airfoil stalls. At the other extreme of the variation of C_L, the lift at α=0 attain a zero value. The surface roughness has a remarkable effect on the aerodynamic characteristics of the tested airfoils. It is noticed clearly from these figures that, the effect of increasing the surface roughness is to decrease the maximum lift coefficient and the critical angle of attack due to earlier flow separation. Massive separation limits the maximum lift coefficient developed by an airfoil and increases the drag coefficient. For example, it is found that, the critical angle of attack for smooth surface is equal to approximately 10 degrees compared with 7 degrees for the higher surface roughness, (RA3). The data also shows that, the angle of zero-lift is practically unaffected by the surface roughness. However, the minimum drag coefficients of rough airfoils occur at an angle of attack approximately equal to α_{cr}, as shown in Figure (33).

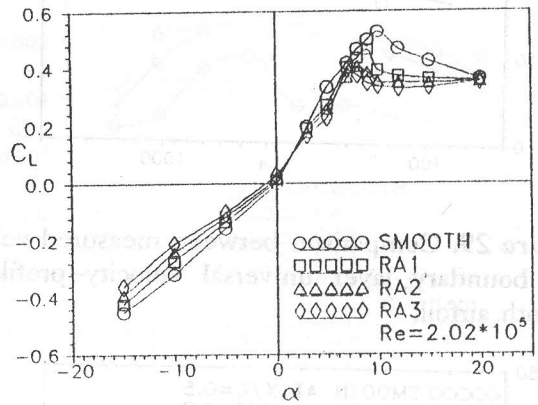

Figure 32. Effect of surface roughness on lift-coefficient distribution.

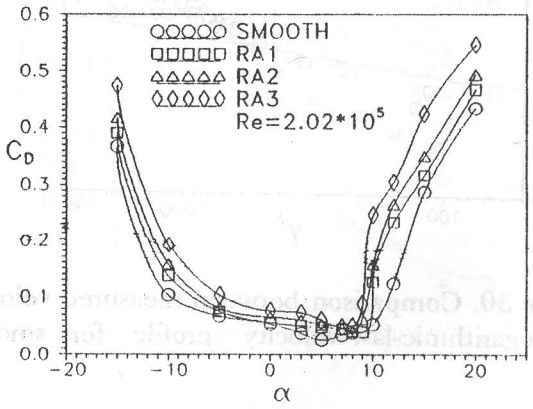

Figure 33. Effect of surface roughness on drag-coefficient distribution.

Usually the function of the airfoil is to produce lift while the drag is connected with the forces necessary to propel the lifting force. Thus, a convenient parameter to measure the effectiveness of an airfoil is its lift-to-drag ratio, C_L/C_D. The maximum value of this quantity gives a good indication of the airfoil effectiveness. For design purposes it is desirable that, this maximum occurs at a high lift coefficient so that the physical size of the lifting surface is minimized. Figures (34) to (36) show the variation in the lift-to-drag ratio, which represent the airfoil performance, with the angle of attack for various roughness at different Reynolds numbers. It is found that, the maximum lift-to-drag ratio and the critical angle of attack are decreased with increasing surface roughness due to increasing of the total drag. Consequently, the operating range of rough airfoil surfaces is limited by stall and separation at low angles of attack.

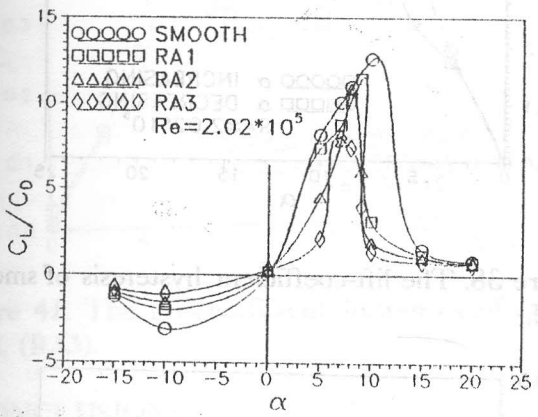

Figure 34. Lift-to-drag ratio of smooth and rough airfoils with angle of attack.

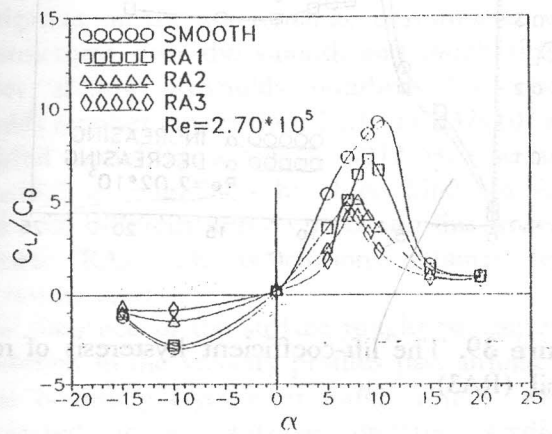

Figure 35. Lift-to-drag ratio of smooth and rough airfoils with angle of attack.

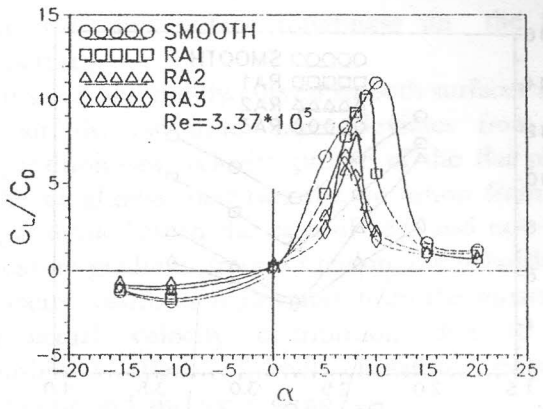

Figure 36. Lift-to-drag ratio of smooth and rough airfoils with angle of attack.

The effect of Reynolds number on the maximum lift-to-drag ratio, (C_L/C_D), is presented in Figure (37) for smooth and rough airfoil surfaces. It is observed from this figure that, the maximum lift-to-drag ratio which gives a good airfoil performance is strongly dependent upon the surface roughness and Reynolds number. The effect of increasing the surface roughness tends to decrease the maximum lift-to-drag ratio. The rate of decrease of this ratio due to the surface roughness is dependent on the Reynolds number. On the other hand, the effect of increasing Reynolds number is to decrease the maximum lift-to-drag ratio of smooth and rough airfoil surfaces up to $R_c = 2.7 \times 10^5$, and then the maximum lift-to-drag. ratio increases with increasing Reynolds number. This can be explained as follows. At low Reynolds number, the viscous effects are relatively large which cause a large drag that limits the maximum lift, while at the higher values of Reynolds number the lift-to-drag ratio is improved due to the high momentum transport. In the presence of surface roughness, a thick turbulent boundary layer suffers from separation or at least causes an additional raising of drag which reduces the airfoil performance. It appears from Figure (37) that, the critical Reynolds number for both smooth and rough airfoils at which improvement of the performance takes place is equal to 2.7×10^5.

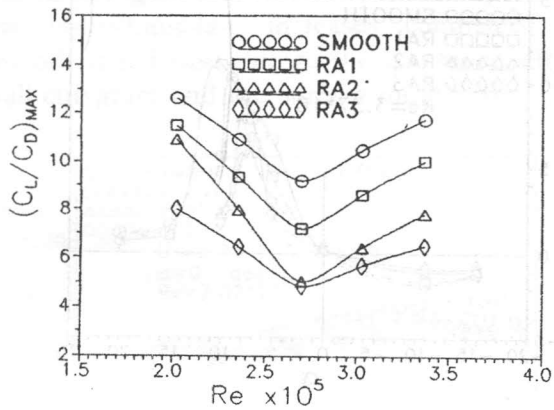

Figure 37. Effect of Reynolds number on the maximum lift-to-drag ratio of smooth and rough airfoils.

The phenomenon of the so-called the lift curves hysteresis is examined for smooth and rough airfoils to obtain the corrected lift coefficient. The occurrence of the hysteresis phenomenon is attributed to the formation and the sudden breakdown or bursting of the leading-edge separation bubble. For the process of increasing angle of attack from lower value, a laminar separation bubble is formed on the upper surface. It then moves upward and shrinks its size accordingly. The turbulent separation point moves toward the leading edge. The stall occurs when the turbulent separation point subsequently meets the bubble. At this moment, the bubble is destroyed and the reattachment no longer exists, this is explained in Ref. [18]. The lift curve is acquired in the process when the change of the angle of attack is increased up to full stall. The process is then reversed until the zero-degree angle of attack is reached where the laminar separation is not restored immediately. Samples of the results for smooth and the more rough airfoil surface (RA3) are presented in Figure (38) and Figure (39) at Reynolds number of 2.02 x 10^5, while Figure (40) and Figure (41) show the same effect at Re = 3.37 x 10^5. The results show that the hysteresis phenomenon is more appreciable in the lift-curves of the smooth airfoil; especially at Reynolds number of 3.37x10^5 where the maximum lift coefficient is dropped by about 20%, as shown in Figure (40). However, for the case of rough airfoil surface, as shown in Figure (41), the hysteresis in the lift coefficient is reduced. It can be observed from these figures also that, the Reynolds number has a significant effect on the hysteresis phenomenon in the case of both smooth and rough airfoils. Therefore, it can be concluded that, hysteresis is of practical importance because it results in producing different aerodynamic performance.

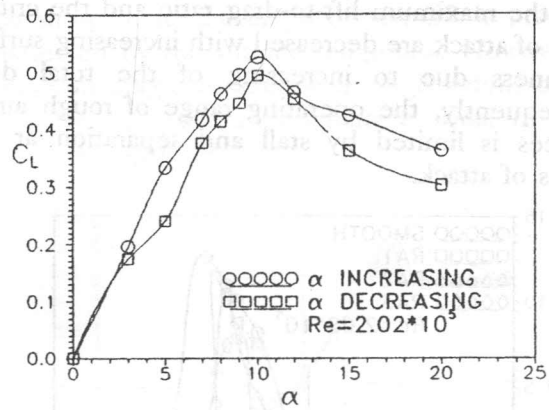

Figure 38. The lift-coefficient hysteresis of smooth airfoil.

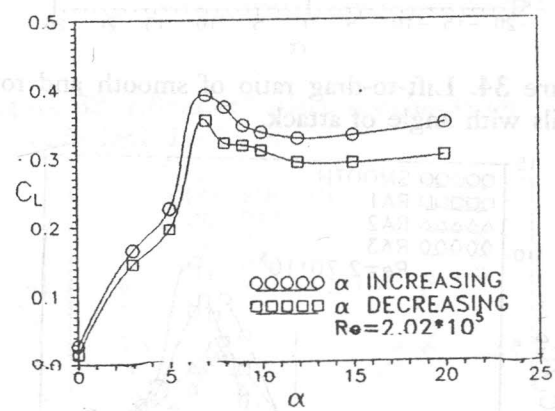

Figure 39. The lift-coefficient hysteresis of rough airfoil, (RA3).

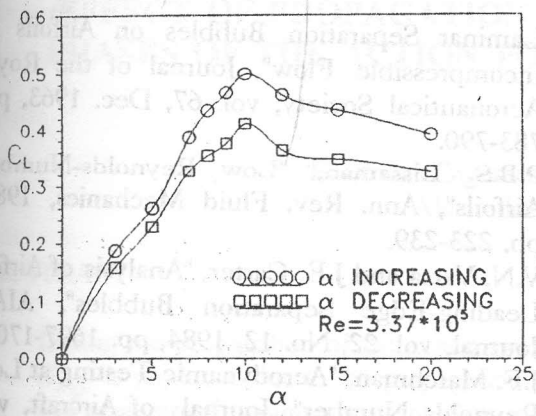

Figure 40. The lift-coefficient hysteresis of smooth airfoil.

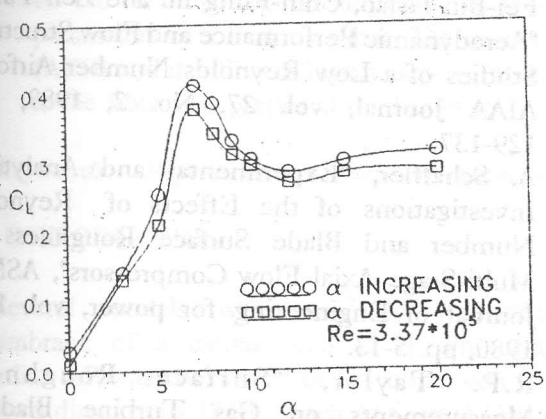

Figure 41. The lift-coefficient hysteresis of rough airfoil, (RA3).

4- CONCLUSIONS

This paper reports the results of an experimental investigation on the aerodynamic performance and flow structures over the smooth and rough airfoils surfaces at low Reynolds number. The chord Reynolds number ranges from $2x10^5$ to $3.37x10^5$ and the airfoil model has a NACA- 0012 cross section. The airfoil is roughened by three kinds of sand papers with different arithmetic center-line average roughness (RA) . The conclusions obtained from these results are :

1- The presence of the surface roughness causes a distortion in the velocity profiles past airfoils.

2- The boundary layer over rough airfoils, when subjected to an adverse pressure gradient ultimately grows more rapidly and separates earlier than that over the smooth airfoil. This occurs due to the combined effects of streamline curvature and surface roughness on the flow structures.

3- For small and mildly curved smooth surfaces such as airfoils, the inner layer deviates from the logarithmic-law velocity profile of the flat plate. The roughness increases the deviation from the logarithmic-law in the case of zero and non-zero pressure gradient. In outer region, the logarithmic velocity distribution deviates from the measured or actual velocity distribution due to the combined effect of wall curvature, pressure gradient and surface roughness.

4- The skin friction coefficient increases with increasing the surface roughness in zero-pressure gradient. On the contrary, the presence of the pressure gradient reduces the skin friction coefficient of rough airfoils.

5- The maximum lift-to-drag ratio, which represents the airfoil performance, decreases with increasing the roughness of the airfoil surface. The critical angle of attack decreases with increasing the surface roughness. Therefore, the operating range of rough airfoil surface is limited by stall and separation at low angles of attack.

6- The angle of zero-lift is particularly unaffected by the surface roughness. However, the minimum drag coefficients of rough airfoils occur at an angle of attack, approximately, equal to the critical angle of attack.

7- The maximum lift-to-drag ratio is dependent upon the Reynolds number and the surface roughness.

8- The hysteresis phenomenon in the lift coefficient-curves of both smooth and rough airfoils is strongly affected by the surface roughness and the operating Reynolds number.

REFERENCES

[1] T. Cebeci, "Wall Curvature and Transition Effects in Turbulent Boundary layers", AIAA Journal, vol. 9, Sept. 1971, pp. 1868-1870.

[2] R.M.C. So and G.L. Mellor, "Experiments on Convex Curvature Effects in Turbulent Boundary layers", Journal of Fluid Mechanics, vol. 60, 1973, pp. 43-62.

[3] R.M.C. So and G.L. Mellor, "Experiments on

Turbulent Boundary Layers on a Concave Wall", Aeronautical Quarterly, vol. XXVI, 1975, pp. 35 - 40.

[4] B.R. Ramaprian and B.G. Shivaprasad, "Mean flow Measurements in Turbulent Boundary Layers along Mildly Curved Surfaces", AIAA Journal, vol. 15, NO. 2, Feb. 1977, pp. 189 - 196.

[5] F.A. Dvorak, "Calculation of Turbulent Boundary Layers on Rough Surfaces in Pressure Gradient", AIAA Journal, vol. 7, Sept. 1969, pp. 1752-1759.

[6] R.A. Antonia and R.E. Luxton, "The Response of a Turbulent Boundary Layer to a Step Change in Surface Roughness", part 1. smooth to Rough, Journal of fluid Mechanics, vol. 48, part 4, 1971, pp. 721-761.

[7] Tuncer Cebeci and K.C. Chang, "Calculation of Incompressible Rough Wall Boundary Layer Flows", AIAA Journal , vol. 16, No. 7, July 1978, pp. 730-375.

[8] K. Yang-Moon, " Turbulent Flow Near a Rough Wall", ASME Journal of fluid Engineering, vol. 114, Dec. 1992, pp. 537-542.

[9] Byung Nam kin and Myung Kyoon Chung," Experimental Study of Roughness Effects on the Separated Flow Over a Backward- Facing Step", AIAA Journal, vol. 33, No. 1, 1994, pp. 159-161.

[10] M. Acharya, J. Bornstein and M.P. Escudier, "Turbulent Boundary Layers on Rough Surfaces", Experiments in Fluids, vol. 4, Jan. 1986, pp. 33-47.

[11] W.J. Feiereisen and M. Acharya, "Modeling of Transition and Surface Roughness Effects on Boundary Layer Flows", AIAA Journal, vol. 24, No. 10, Oct. 1986, pp. 1642 - 1649.

[12] B.J. Abu-Ghanam and R. show, "Natural Transition of Boundary Layer- The Effect of Turbulence, Pressure Gradient and Flow History", Journal of Mechanical Engineering Science , vol. 20, No. 5, 1980, pp. 213-228.

[13] M.F. Blair, "Influence of Free-Stream Turbulence on Boundary Layer Transition in Favorable Pressure Gradient", ASME Journal of Engineering for Power, vol. 104, 1982, pp. 743-750.

[14] J.W. Ward, "The Behavior and Effects of Laminar Separation Bubbles on Airfoils Incompressible Flow", Journal of the Roy Aeronautical Society, vol. 67, Dec. 1963, p 783-790.

[15] P.B.S. Lissaman, "Low Reynolds-Numbe Airfoils", Ann. Rev. Fluid Mechanics, 198 pp. 223-239.

[16] V.N. Vatsa and J.E. Carter, "Analysis of Airfoi Leading-Edge Separation Bubbles", AIA Journal, vol. 22, No. 12, 1984, pp. 1697-1704

[17] J.F. Marchman, "Aerodynamic Testing at Lov Reynolds Number", Journal of Aircraft, vol 24, Feb. 1987, pp. 107-114.

[18] Fei-Bin Hsiao, Chin-Fung liu and Zen Tung "Aerodynamic Performance and Flow Structure Studies of a Low Reynolds Number Airfoil", AIAA Journal, vol. 27, No. 2, 1989, pp. 129-137.

[19] A. Schaffler, "Experimental and Analytical Investigations of the Effects of Reynolds Number and Blade Surface Roughness of Multi-Stage Axial Flow Compressors", ASME Journal of Engineering for power, vol. 102, 1980, pp. 5-13.

[20] R.P. Taylor, "Surface Roughness Measurements on Gas Turbine Blades", ASME, Journal of Turbomachinery, vol. 11, 1990, pp. 175-180.

[21] J.C. Gibbings, O.T. Goksel and D.J. Hall, "The Influence of Roughness Trips Upon the Boundary Layer Transition", part 1. Characteristics of wire trips, Aeronautical Journal, 1968, pp. 289-301.

[22] J.C. Gibbings, O.T. Goksel and D.J. Hall, "The Influence of Roughness Trips Upon the Boundary Layer Transition" Part 2. Characteristics of Single Spherical Trips, Aeronautical Journal, 1968, pp. 357-.

[23] F.H. Clauser, "The Turbulent Boundary Layer", Advances in Appl. Mech. 4, Academic Press, 1956.

[24] S.J. Kline and F.A. McClintack, "Describing the Uncertainties in Single-Sample Experiments", ASME Mechanical Engineering Journal, Jan. 1953, pp. 3-8..

[25] H. Schlichting, "Boundary-Layer Theory", 6 th. ed., 1968, McGraw-Hill, New-York.